Tuning the Spin Interaction in Nonplanar Organic Diradicals through Mechanical Manipulation

Vegliante, Alessio; Fernández, Saleta; Ortiz, Ricardo; Vilas-Varela, Manuel; Baum, Thomas Y.; van der Zant, Herre S.J.; Frederiksen, Thomas; Peña, Diego; Pascual, Jose Ignacio; More Authors

DOI
10.1021/acsnano.4c01963

Publication date
2024

Document Version
Final published version

Published in
ACS Nano

ACS NANO

www.acsnano.org

ARTICLE

Tuning the Spin Interaction in Nonplanar Organic Diradicals through Mechanical Manipulation

Alessio Vegliante, Saleta Fernández, Ricardo Ortiz, Manuel Vilas-Varela, Thomas Y. Baum, Niklas Friedrich, Francisco Romero-Lara, Andrea Aguirre, Katerina Vaxevani, Dongfei Wang, Carlos Garcia Fernandez, Herre S. J. van der Zant, Thomas Frederiksen,* Diego Peña,* and Jose Ignacio Pascual*

Cite This: *ACS Nano* 2024, 18, 26514–26521

Read Online

ACCESS | Metrics & More | Article Recommendations | Supporting Information

ABSTRACT: **Open-shell polycyclic aromatic hydrocarbons (PAHs) represent promising building blocks for carbon-based functional magnetic materials. Their magnetic properties stem from the presence of unpaired electrons localized in radical states of π character. Consequently, these materials are inclined to exhibit spin delocalization, form extended collective states, and respond to the flexibility of the molecular backbones. However, they are also highly reactive, requiring structural strategies to protect the radical states from reacting with the environment. Here, we demonstrate that the open-shell ground state of the diradical 2-OS survives on a Au(111) substrate as a global singlet formed by two unpaired electrons with antiparallel spins coupled through a conformational-dependent interaction. The 2-OS molecule is a "protected" derivative of the Chichibabin's diradical, featuring a nonplanar geometry that destabilizes the closed-shell quinoidal structure. Using scanning tunneling microscopy (STM), we localized the two interacting spins at the molecular edges, and detected an excited triplet state a few millielectronvolts above the singlet ground state. Mean-field Hubbard simulations reveal that the exchange coupling between the two spins strongly depends on the torsional angles between the different molecular moieties, suggesting the possibility of influencing the molecule's magnetic state through structural changes. This was demonstrated here using the STM tip to manipulate the molecular conformation, while simultaneously detecting changes in the spin excitation spectrum. Our work suggests the potential of these PAHs as all-carbon spin-crossover materials.**

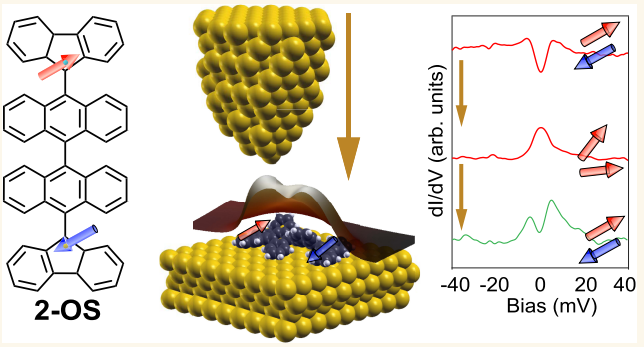

KEYWORDS: *organic diradicals, carbon magnetism, on-surface synthesis, exchange coupling, scanning tunneling microscopy*

Carbon-based molecular nanostructures can exhibit magnetic states associated with the stabilization of unpaired electrons in radical sites.[1] Intrinsic π-magnetism has been widely observed in polycyclic aromatic hydrocarbons (PAHs) with an open-shell ground state, i.e., possessing one or more unpaired π electrons.[2−5] Compared to traditional inorganic materials, the magnetism associated with these systems features longer spin coherence times and more delocalized magnetic moments, combined with a high degree of chemical and mechanical tunability.[6−8] In this context, organic diradicals are of fundamental interest for understanding magnetic interactions at the molecular scale and developing control strategies.[9] Overall, open-shell organic systems have great potential for applications in diverse technologies such as sensorics, nonlinear optics, or spintronics.[10−15]

A classical example of open-shell PAH is the Chichibabin's hydrocarbon, a molecule that has been extensively investigated for its large diradical character in the ground state.[16,17] To circumvent its high reactivity, several derivatives have been

Received: February 8, 2024
Revised: August 21, 2024
Accepted: August 22, 2024
Published: September 20, 2024

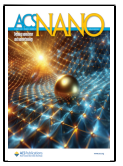

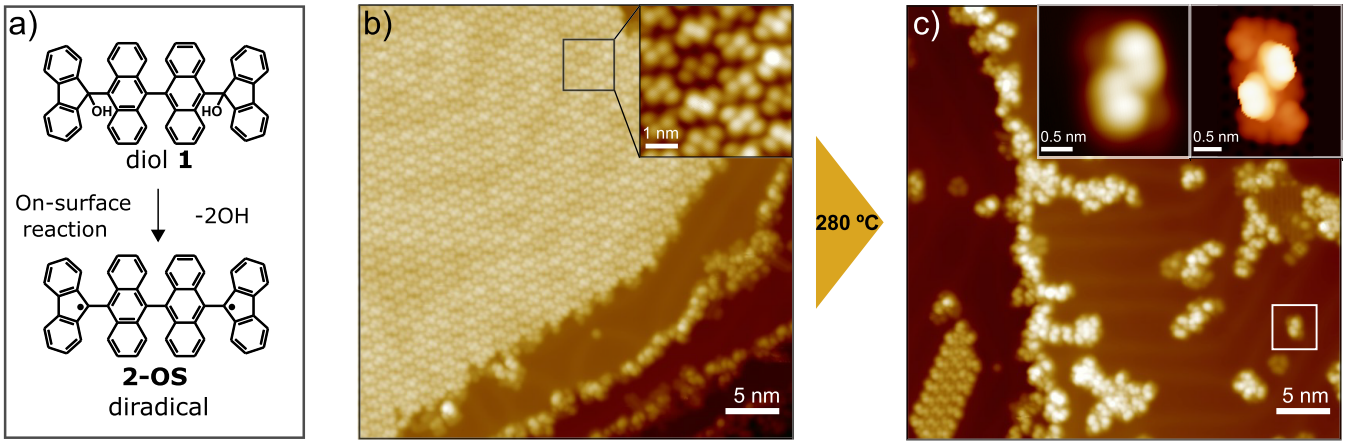

Figure 1. (a) Schematic representation of the generation of the 2-OS diradical through dissociation of the OH groups from the diol 1 deposited on the Au(111) substrate. (b) Overview STM constant-current image displaying the typical close-packed domain formed by the molecular precursors when deposited on the Au(111) surface (V = −1.25 V; I = 46 pA). In the inset, close-packed structure showing the arrangement and the shape of the individual molecules (V = −1.25 V; I = 30 pA). (c) STM constant-current image recorded after annealing the sample at 280 °C (V = −1.25 V; I = 30 pA). In the inset: left, STM image of a single isolated molecule as found after the annealing (V = −1.25 V; I = 30 pA); right, DFT charge density calculation of 2-OS on Au(111).

prepared, one of the latest examples being a stable compound reported by Zeng et al. (**2-OS**, Figure 1a).[18] The **2-OS** molecule consists of a central bisanthracene unit linked to two fluorenyl termini that accumulate the radical character of the system. The steric hindrance between fluorenyl and anthracene moieties determines a highly nonplanar structure that is responsible for the protection of the radical centers, which remain localized over the fluorenyl subunits. Owing to high stability of its diradical ground state and its tunable nonplanar structure, **2-OS** is a suitable system to explore the relationship between magnetism and geometry at the single molecule scale.

A triplet ground state has been reported for **2-OS** in solution, in agreement with density functional theory (DFT) calculations of the magnetic state of the molecule in the gas phase.[18] Recently, **2-OS** has also been studied in mechanically controlled break-junction devices,[19] where spectroscopic features of either the singlet or triplet ground state have been detected. These variations in the sign of the magnetic exchange have been attributed to different torsional angles between the different conjugated moieties,[19] enhanced by the contacts to metallic terminals,[20] but a clear demonstration of the correlation between magnetic exchange and structure is lacking.

Here, we demonstrate that the spin−spin coupling in the **2-OS** diradical can be manipulated by modifying its conformational structure. Low-temperature scanning tunneling microscopy (STM) and spectroscopy (STS) measurements show that the open-shell character of **2-OS** persists on a Au(111) substrate with a singlet ground state very close in energy to a triplet excited state. Mean-Field Hubbard simulations reveal the influence of molecular geometry on the exchange coupling between the radical centers. Following these findings, we demonstrate the possibility of tuning the spin state of the molecule by modifying the arrangement of its constituent units through mechanical manipulation with the STM tip.

RESULTS AND DISCUSSION

On-Surface Generation and Characterization of 2-OS.

Evaporating di- and poly radicals onto a substrate is known to be particularly challenging, as it easily results in fragmentation due to thermal instability.[21,22] In order to get intact **2-OS** molecules on a Au(111) surface, we sublimated diol **1**, a stable molecular precursor containing a hydroxyl group (OH) capping each of the two radical centers at the fluorenyl termini, and subsequently induced an on-surface reaction to dissociate the OH groups and generate **2-OS**, as shown schematically in Figure 1a.

The diol **1** was evaporated onto a clean Au(111) surface under ultrahigh vacuum (UHV) conditions. Extended close-packed molecular domains were found on the Au surface after the sublimation, as revealed by constant-current STM images (Figure 1b). A closer look into these structures shows that the constituent molecules appear partially planarized, and display four lobes: the two internal ones can be attributed to the anthracene units and the ones at the ends to the fluorenyl termini. Differential conductance (dI/dV) spectra acquired on the molecules inside the close-packed structures show no fingerprints of magnetism (Supporting Information, Figure S7). This is expected as a consequence of the presence of the OH groups of compound **1**, that are not detached upon deposition onto the surface and still passivate the radical centers, preserving the closed-shell structure of the precursor.

The sample was thus annealed with the aim of inducing the C−OH cleavage, in a similar manner to the deoxygenation reaction previously described for epoxyacene derivatives.[23] Figure 1c shows an overview after annealing at 280 °C: some close-packed domains of reduced dimensions can still be seen, alongside single isolated molecules, chains and small molecular clusters of several shapes. Individual molecules appear in constant-current STM images as shown in the inset in Figure 1c: they feature two internal brighter lobes, that can be attributed to the anthracene moieties, and darker external features, corresponding to the fluorenyl termini. A more detailed elucidation of the molecular structure with bond resolution is hindered by the nonplanarity of the system. However, our DFT simulations of the charge density of **2-OS** on the Au(111) surface (also reported in Figure 1c) is in good agreement with the main features found in the STM topography, confirming our identification of the individual molecules.

https://doi.org/10.1021/acsnano.4c01963
ACS Nano 2024, 18, 26514−26521

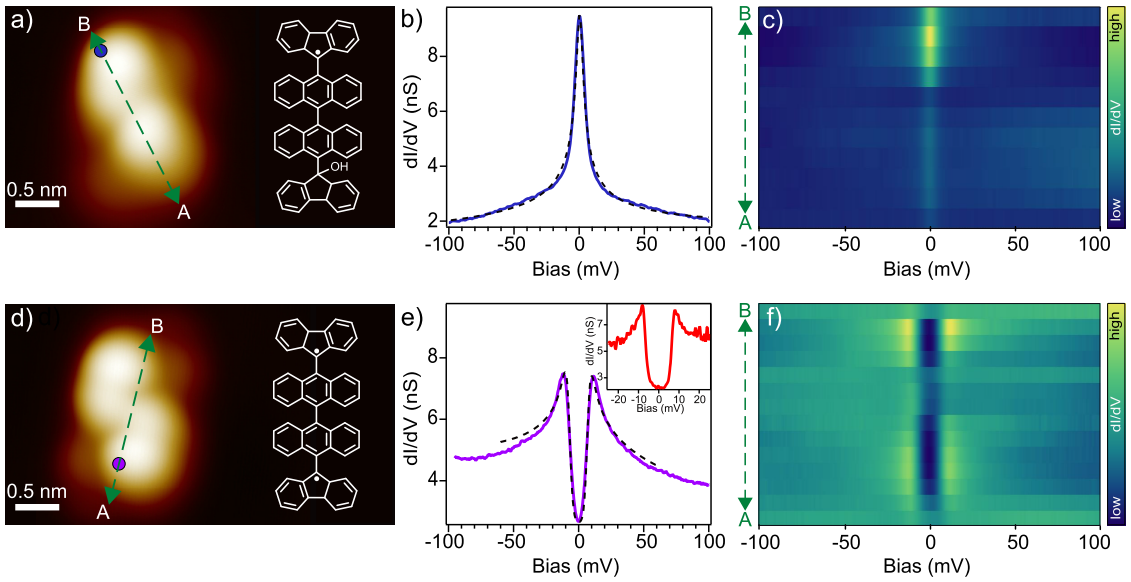

Figure 2. (a, d) STM constant-current images (V = −1.25 V; I = 30 pA) of single molecules as found after the on-surface reaction and the corresponding molecular structures, in the two configurations: (a) with a residual OH group, corresponding to a monoradical, and (d) with no OH groups, corresponding to the 2-OS diradical. (b) dI/dV spectrum taken on the molecule in (a) at the position indicated by the blue circle, displaying a zero-bias resonance, that can be fitted with a Frota function (black dashed line).[24] (c) dI/dV linescan measured across the molecule in (a) in the direction indicated by the arrow (V = −200 mV, I_{set} = 500 pA, V_{mod} = 2 mV). (e) dI/dV spectrum measured on the molecule in (d) at the position indicated by the purple circle, showing spin excitation steps. The black dashed line represents fits to the data using the perturbative model by Ternes,[25] from which an antiferromagnetic exchange J = 7.3 meV is obtained. The inset shows a spectrum measured at T = 1.3 K, emphasizing the IET gap (V = 30 mV, I_{set} = 200 pA, V_{mod} = 0.8 mV). (f) dI/dV line spectra measured across the molecule in (d) in the direction indicated by the arrow (V = −100 mV, I_{set} = 500 pA, V_{mod} = 2 mV).

An alternative approach for the on-surface formation of **2-OS** consists in inducing the C−OH cleavage by means of a voltage pulse, obtained by placing the tip on top of a molecule and raising the sample positive bias above 1.5 V. As shown in the Supporting Information (Figure S8), this procedure allows to remove one or more OH groups in the same molecule or in a neighboring molecule within the assembled domains and molecular clusters, but does not provide isolated molecules over the substrate. Therefore, our further analysis is based on single molecules obtained by annealing the substrate.

Two distinct molecular structures are generally found after the annealing step, corresponding to one or both OH groups detached following the on-surface reaction (Figure 2a,d). The STM constant-current images appear roughly the same in the two cases; nevertheless, scanning tunneling spectroscopy allows the identification of two distinct spin states, that can be related to the two configurations with different numbers of OH groups left.

In a fraction of molecules (around 25% of the single molecules that have been investigated, Figure 2a), the dI/dV spectra display a pronounced zero-bias peak, as depicted in Figure 2b. This feature is well reproduced by a Frota function with HWHM = 6.1 meV, and can be attributed to a Kondo resonance, arising from the screening of a localized spin S = 1/2 by the conduction electrons of the metal substrate.[3,24,26−28] The dI/dV stacked plot taken along an axis of the molecule (Figure 2c) shows that the Kondo resonance is not spatially homogeneous but significantly more intense in one-half of the molecule. We relate this spin state to a monoradical structure in which one OH group persists after the annealing and therefore conclude that the Kondo resonance is associated with the single unpaired electron recovered from the partial OH dissociation.

However, most of the individual molecules found after annealing (Figure 2d) display a distinct low-energy feature consisting of a narrow gap centered at zero-bias, followed by two sharp dI/dV peaks at ±11 meV, as depicted in Figure 2e. The dI/dV stacked plot in Figure 2f reveals that these features appear distributed all over the molecule, weaker over the center of the molecule but with higher amplitude toward the fluorenyl end-groups. Based on the symmetric position of the dI/dV peaks, we attribute these features to an inelastic electron tunnelling (IET) excitation of the two exchange-coupled spins at the radical sites,[3,4,29−33] confirming that in this case both OH groups have been detached, activating the **2-OS** diradical.

We note that dI/dV spectra exhibit a higher-bias characteristic falloff, resembling a Kondo resonance superimposed on the gapped spectrum.[3,32] Furthermore, such Kondo-like feature is absent at zero bias (see STS spectrum recorded at 1.3 K in inset in Figure 2e). This indicates that the Kondo-like fluctuations are enabled by inelastic electrons tunneling through the excited state[20,27,34] but are absent in the ground state. The spectral shape can be interpreted as caused by the inelastic excitation of a singlet (total spin S = 0) ground state into a triplet (S = 1) excited state. A model of two antiferromagnetically coupled S = 1/2 spins[25] (dashed line in Figure 2e) reproduces well the spectral features, revealing an exchange interaction between the flourenyl moieties of $J \sim 7.3$ meV. Therefore, we conclude that **2-OS** exhibits a singlet ground state on a Au(111) surface, excluding the previously observed triplet ground state,[18] since this would result in a very different spectral line shape.

Theoretical Calculations. To explain the origin of the antiferromagnetic coupling found on the Au substrate, we performed tight-binding mean-field Hubbard (TB-MFH) simulations of the magnetic ground state of **2-OS** in different

https://doi.org/10.1021/acsnano.4c01963
ACS Nano 2024, 18, 26514−26521

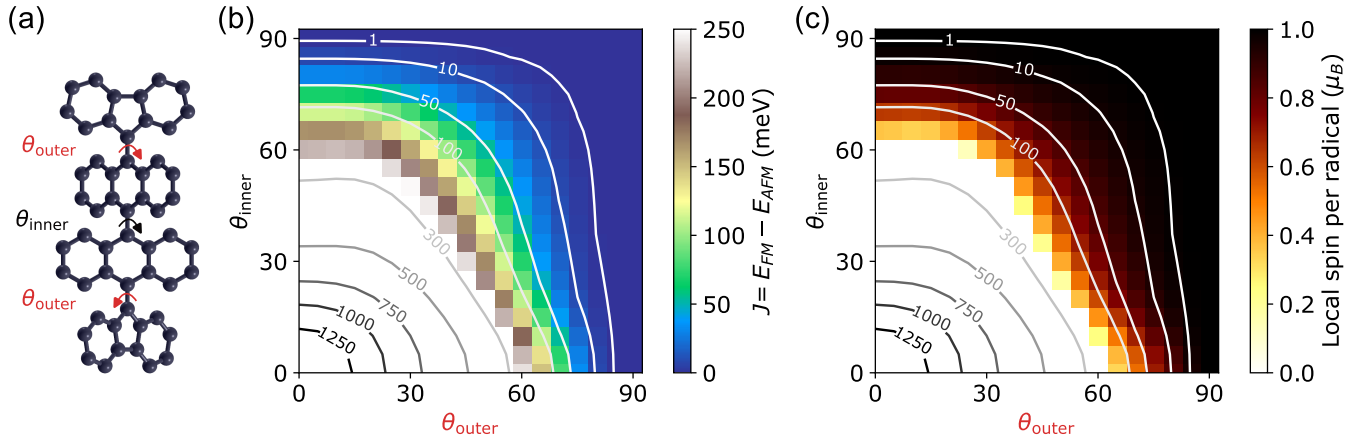

Figure 3. TB-MFH calculations for the exchange coupling as a function of torsional angles in 2-OS. (a) Structural model for the 2-OS carbon backbone with three torsional angles. For simplicity, we fix the two outer angles θ_{outer} to be identical. (b) MFH results for the intramolecular exchange coupling $J = E_{FM} - E_{AFM}$ between the two radicals, obtained using a value of $U = 3$ eV,[35] as a function of the two torsional angles θ_{outer} and θ_{inner}. The value of J is obtained as the energy difference between ferromagnetic (FM) (solution constrained to $S_z = 1$) and antiferromagnetic (AFM) order (solution constrained to $S_z = 0$). The contours represent constant-J in meV: the AFM solution is always the ground state, but J approaches zero whenever one of the two angles reaches 90°. (c) Local spin polarization per radical (defined as the sum of the spin density over sites on one-half of the molecule) in the AFM state, as a function of the two torsional angles θ_{outer} and θ_{inner}. The constant-J contours from (b) are also included here as a guide. For $J \gtrsim 200$ meV the ground state becomes a closed-shell singlet (no local polarization).

geometries. Specifically, we calculated the energy of the antiferromagnetic (AFM, the singlet case) spin arrangement with respect to the ferromagnetic (FM, the triplet solution) case, i.e., $J = E_{FM} - E_{AFM}$, as a function of the dihedral angles θ_{inner} (between the central anthracenes) and θ_{outer} (between each anthracene and the outer fluorenyl). For simplicity, we assumed the two outer angles to be identical and the individual anthracenes and fluorenyls units to be planar. We considered a single p-orbital per carbon site, locally perpendicular to the backbone unit and constructed the corresponding TB Hamiltonian with SISL[36] using the Slater–Koster parameterization of ref 37 (see Supporting Information Section 3.1).

The variation of J as a function of the two torsional angles is depicted in Figure 3b. The singlet is always the ground state for any combination of θ_{inner} and θ_{outer}. However, we observe a clear trend in the evolution of J with the conformation: its value is close to 0 when any of the torsional angles approach 90°, but it progressively increases as the angles reduce. This means that the planarization of the molecular structure (i.e., the decrease of the angles between the units) stabilizes the singlet solution, unveiling an increasingly higher AFM exchange coupling. According to the TB-MFH results shown in Figure 3c, the effect of planarization is drastic: the spin polarization vanishes for angles below 60°, revealing that for smaller angles, the open-shell singlet transforms itself into a (spin-unpolarized) closed-shell singlet.

The experimental observation of a singlet ground state for **2-OS** on Au(111) is in agreement with the trend obtained in the MFH simulations. The interaction with the flat metal substrate is expected to induce a partial planarization of the molecular units (see the DFT calculation of the adsorption geometry in Supporting Information, Section 3.2), contributing to the stabilization of the AFM order. From TB-MFH results, the FM solution is always less energetically favorable than the AFM one, even for high values of the torsional angles. This apparently contradicts results from previous DFT calculations, which found a triplet ground state in the gas phase, with a triplet-singlet gap of 26 meV.[18] This discrepancy is explained by considering that the value reported by Zeng et al.[18] takes into account also vibrational effects due to temperature. Including these in our DFT simulations, we reproduced the higher stability of the triplet ground state for a gas-phase relaxed molecule (i.e., with both angles $\theta_i \sim 90°$) and at room temperature (shown in Supporting Information, Section 3.3). At the lower temperature of our experiment, however, vibrational effects do not play a significant role, and DFT qualitatively reproduces the results of the TB-MFH calculations.

In any scenario, all simulation tools agree that decreasing the torsional angle of the molecular subunits stabilizes the singlet state. As shown in Figures S12 and S13, this can be explained by the increase in hopping elements across the dihedral angles. These matrix elements primarily enhance kinetic exchange mechanisms, which induce AFM ordering in **2-OS**, while direct Hund's-like exchange is expected to be negligible.[20,39,40] Following these theoretical results, the controlled modification of the spin interactions should be achievable by tuning the molecular configuration.

Mechanical Manipulation of the Spin–Spin Coupling. Motivated by the theoretical predictions indicating a correlation between the geometry of **2-OS** and the exchange coupling J, we explored the possibility of modifying its spin excitation gap and magnetic ground state by controllably manipulating the molecular conformation using the STM tip. We note that the nonplanar structure of **2-OS** arises from hindrance among different conjugated units, imposing the persistence of a dihedral angle even on the metal substrate (see Figure S14). Consequently, we anticipated that approaching the STM tip toward the central part of the molecule would exert attractive or repulsive forces over these submolecular units, forcing variations of their dihedral angle,[41,42] as observed in our DFT simulations in Figure S15.

However, due to the weak interaction with the surface, **2-OS** molecules were abruptly modified, and frequently displaced toward the STM tip in response to attractive forces (see Figure S9). To overcome this issue, we designed an extended version

https://doi.org/10.1021/acsnano.4c01963
ACS Nano 2024, 18, 26514–26521

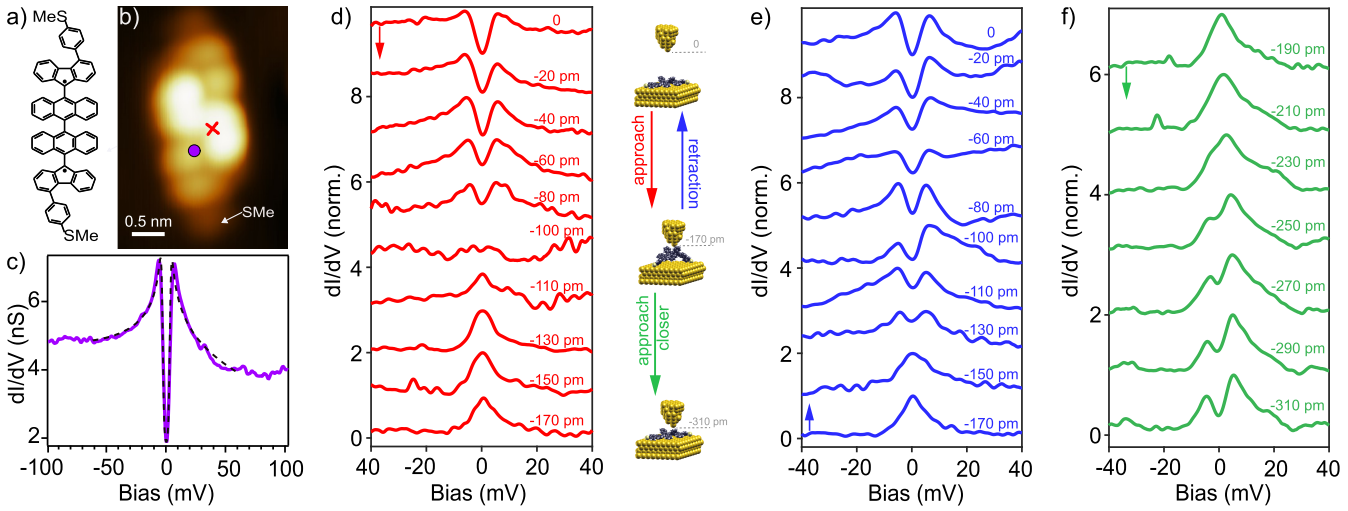

Figure 4. (a) Chemical model of SMe-2OS, the sulfide substituted analogue of 2-OS synthesized for the manipulation experiment. (b) STM image (V = −1.25 V; I = 30 pA) of SMe-2OS, as obtained after the on-surface generation of the diradical, reported in the Supporting Information. (c) dI/dV spectrum measured on the molecule at the position indicated by the purple circle in (b), displaying the same IET feature as 2-OS. The black dashed line is a fit to the data using the perturbative model by Ternes,[25] revealing an antiferromagnetic exchange J = 3 meV. (d–f) Normalized dI/dV plots recorded during the mechanical manipulation of the spin state of SMe-2OS, as indicated in the central scheme. The STM tip is stabilized on the molecule in the position marked by the red cross in (b) at a starting height (here indicated as 0) determined by I = 200 pA and V = 50 mV. dI/dV spectra are measured after approaching the tip by the indicated distances, in three sequences: (d) while approaching the tip down to 170 pm with respect to the starting position; (e) when retracting back toward the starting position; (f) while continuing approaching to lower tip–sample distances from the end of (d). At some positions, a peculiar IET peak asymmetry is observed, attributed to particle-hole asymmetries,[38] probably caused by the coupling to the tip.[31] The dI/dV spectra were normalized following the procedure described in the Methods section. Spectroscopy parameters: V_{mod} = 2 mV, I_{set} = 200 pA.

of the diradical, denoted **SMe-2OS** (Figure 4a), wherein methylthiophenyl moieties were strategically incorporated at each fluorenyl subunit. These moieties were chosen since sulfur groups are widely used for anchoring molecules to gold electrodes.[43−45]

Similar to the **2-OS** base molecule, we generated the **SMe-2OS** diradical on the Au(111) surface by depositing the corresponding closed-shell precursor containing OH protecting groups at the two radical sites (see structure of diol **10** in Figure S1). In this case, we activated the OH decapping by applying controlled bias pulses over the molecular center, as illustrated in Figure S10. The STM constant-current image of the resulting **SMe-2OS** molecule, shown in Figure 4b, reveals similar bulky features like in **2-OS** species but with the addition of two smaller bright lobes at each end, attributed to the methylthiophenyl end groups.

The dI/dV spectra measured on **SMe-2OS** (Figure 4c) reproduce similar features as in **2-OS**, namely, IET onsets attributed to singlet–triplet spin excitation, accompanied by a dI/dV decrease characteristic of Kondo fluctuations in the excited state. This confirms that the addition of the edge groups preserves the magnetic ground state of **2-OS**. The singlet–triplet gap in **SMe-2OS** is ∼3 meV, smaller than in **2-OS**. Owing to the strong sensitivity of the intramolecular exchange with the conformation reported in Figure 3b, the smaller value of J reflects the slightly larger values of torsional angles in the relaxed structure of **SMe-2OS** on gold, probably induced by the bonding of SMe end groups with the substrate.

To study the evolution of spin interactions in **SMe-2OS** as a function of structural changes, we stabilized the STM tip above the center of the molecule (red cross in Figure 4b) and performed dI/dV measurements while the STM tip was approached to or retracted from the molecule in steps of 10 or 20 pm. Figure 4d displays spectra measured while approaching the tip 170 pm from the starting position. The width and depth of the excitation gap decreases along the first approaching steps until collapsing into a zero-bias peak at 100 pm. This change can be interpreted as a transition to a new spin state of **SMe-2OS** caused by the structural modification induced by the STM tip. The approach of a tip to a molecular adsorbate is known to cause attractive forces of tens of piconewtons,[46] which can induce detectable distortions in the structure of the adsorbed molecules.[47,48] In the present case, vertical forces rearrange the internal anthracene units into a less planar conformation, as shown in the schematic representation of Figure 4d. DFT simulations shown in Figure S15 find that the major distortion caused by the approach of an arbitrary STM tip is an increase in both inner and outer dihedral angles. As suggested by the MFH results, an increase in one or both the torsional angles results in the reduction of the intramolecular spin–spin coupling. Therefore, the zero-bias peak observed in the final steps of the approach can be attributed to a Kondo-like feature, emerging when the two spins become non-interacting.

The mechanical manipulation of the spin state of the diradical is reversible (Figure 4e). Retracting the tip back to the starting position restores the initial inelastic spectral features, thus indicating that the molecule is brought back into the original conformation stabilized by the substrate. The reversibility of this process demonstrates that the change in the spectra is caused by mechanical modifications rather than by the formation of a tip-molecule bond (and consequent quenching of a spin).

The antiparallel spin configuration is restored back when the STM tip is moved further toward the molecule from the closest point in Figure 4d. Figure 4f shows dI/dV spectra measured while approaching the tip 190 to 310 pm with respect to the starting position in Figure 4d. In this range, the Kondo peak

https://doi.org/10.1021/acsnano.4c01963
ACS Nano 2024, 18, 26514−26521

gradually develops a gap, opening as the STM tip approaches, attributed to the reactivation of an inelastic spin excitation. This indicates that the molecule is gradually pushed back toward the substrate, progressively restoring the original torsional angles between the central anthracenes and recovering the antiparallel spin interaction. This agrees with previous noncontact AFM results,[46] which revealed that attractive forces in the tip−sample junction persist for about 300 pm of tip approach before entering a regime of repulsive interactions. Curiously, this gap-reopening is smooth, in contrast to the first range of the approach (Figure 4d), where a sudden gap closing occurred. This suggests that the dihedral angle can be tuned gradually in the range of pushing, while during the initial pulling regime, the attractive forces acting at larger distances induce a more sudden structural reorganization. The more gradual transition in this range, and the comparison with the initial approach/retraction can be also visualized in the computed d^2I/dV^2 spectra reported in Figure S11, where we indicate the spin excitation gaps.

These results demonstrate that the spin−spin coupling in **2-OS** can be tuned utilizing mechanical manipulation reversibly, confirming the theoretical prediction of a strong interplay between precise structural conformation and magnetic state.

CONCLUSIONS

In summary, we have demonstrated that the Chichibabin's hydrocarbon **2-OS** retains its open-shell character on a Au(111) surface with a singlet ground state consisting of two antiparallel aligned spins. Through the cleavage of protecting groups of the deposited diol precursors followed by spatially resolved scanning tunneling spectroscopy measurements, we resolved singlet−triplet excitations at the energy $J \sim 7.3$ meV, thus quantifying their exchange coupling strength. Theoretical MFH simulations found that the substrate-induced partial planarization of **2-OS** favors the antiparallel coupling of the unpaired π electrons, while increasing the torsional angle between the molecular moieties progressively reduces the spin exchange coupling. The ability to tailor magnetic interactions by torsional forces is a promising avenue for the realization of molecule-based sensors. Therefore, we demonstrated this possibility using a **2-OS** molecule functionalized with anchoring end groups, which fix the molecule to the metal while inducing structural modifications with the STM tip. We observed that the spin−spin interaction decreases when the molecule is partially lifted from the substrate (thus acquiring a more orthogonal conformation), and that the initial singlet state can be recovered when bringing it back to a more planar arrangement. The robust singlet ground state found at low temperature contrasts with the triplet ground state found at room temperature.[18] We attributed this temperature dependence to the contributions of thermally excited vibrational deformations. Together with the reported high sensitivity of the magnetic ground state of these Chichibabin's hydrocarbons to mechanical interactions, our results suggest a strong potential of **2-OS** as an all-organic spin-cross over material.

METHODS

The (111) surface of a single Au crystal was cleaned by several cycles of sputtering with Ne gas and successive annealing at $T = 600$ °C under UHV conditions. The precursors of **2-OS** and **SMe-2OS** were prepared in solution following the protocol described in the Supporting Information (Section 1) and evaporated onto the Au(111) surface held at room temperature. The sublimation of intact precursor molecules can be achieved via fast thermal heating of a silicon wafer loaded with grains of the compound, as well as through a standard Knudsen cell. All the measurements were performed in a custom-made low-temperature STM at 5 K in UHV, with the exception of the dI/dV spectrum in the inset of Figure 2e, measured in a commercial Joule-Thompson (JT) STM with a base temperature of 1.3 K.

Differential conductance spectra were recorded using a lock-in amplifier with frequency $f = 867.9$ Hz (Figure 2) and $f = 944$ Hz (Figure 4), with the modulation amplitude and current parameters indicated in the text.

The distance-dependent dI/dV measurements reported in Figure 4d−f were performed by stabilizing the tip on top of a molecule with the set point parameters indicated in the text and using a custom-built interface to control the tip movement z and simultaneously record the tip movement, the current, the bias and the lock-in signal. The spectra displayed in Figure 4d−f were obtained after subtracting a third order polynomial background adjusted to each spectrum and then normalizing the conductance between the maximum and minimum value, according to the formula $G_{norm}(V) = (G(V) - G_{min})/(G_{max} - G_{min})$, where $G(V)$ is the differential conductance at bias V, and G_{max} and G_{min} the maximum and minimum value of $G(V)$ respectively. All STM images and dI/dV spectra were performed with gold-coated tungsten tips. The Figures representing experimental data were prepared using WSxM and SpectraFox softwares.[49,50]

The TB-MFH simulations in Figure 3 and the DFT calculations explained in the Supporting Information (Section 3) were realized using the software packages HUBBARD,[35] SISL,[36] GAUSSIAN[51] and SIESTA.[52]

ASSOCIATED CONTENT

Supporting Information

The Supporting Information is available free of charge at https://pubs.acs.org/doi/10.1021/acsnano.4c01963.

Detailed synthetic description of the molecular precursors of **2-OS** and **SMe-2OS**, and corresponding spectroscopic data; additional STM and STS data: sample after deposition of diol **1**, on-surface generation of **2-OS** by tip-induced reactions, manipulation experiments on **2-OS**, on-surface generation of **SMe-2OS**, computed derivative of the dI/dV spectra in Figure 4; complementary MFH calculations; DFT study of the adsorption geometry of **2-OS** on Au(111) and of the changes due to interactions with the STM tip, and DFT calculations including the effects of temperature (PDF)

AUTHOR INFORMATION

Corresponding Authors

Thomas Frederiksen − *Donostia International Physics Center (DIPC), 20018 Donostia-San Sebastián, Spain; IKERBASQUE, Basque Foundation for Science, 48013 Bilbao, Spain;* orcid.org/0000-0001-7523-7641; Email: thomas_frederiksen@ehu.eus

Diego Peña − *Centro Singular de Investigación en Química Biolóxica e Materiais Moleculares (CiQUS) and Departamento de Química Orgánica, Universidade de Santiago de Compostela, 15782 Santiago de Compostela, Spain;* orcid.org/0000-0003-3814-589X; Email: diego.pena@usc.es

Jose Ignacio Pascual − *CIC nanoGUNE-BRTA, 20018 Donostia-San Sebastián, Spain; IKERBASQUE, Basque Foundation for Science, 48013 Bilbao, Spain;* Email: ji.pascual@nanogune.eu

https://doi.org/10.1021/acsnano.4c01963
ACS Nano 2024, 18, 26514−26521

Authors

Alessio Vegliante − *CIC nanoGUNE-BRTA, 20018 Donostia-San Sebastián, Spain;* orcid.org/0009-0008-6042-5015

Saleta Fernández − *Centro Singular de Investigación en Química Biolóxica e Materiais Moleculares (CiQUS) and Departamento de Química Orgánica, Universidade de Santiago de Compostela, 15782 Santiago de Compostela, Spain;* orcid.org/0000-0002-6282-1694

Ricardo Ortiz − *Donostia International Physics Center (DIPC), 20018 Donostia-San Sebastián, Spain;* orcid.org/0000-0003-3535-0812

Manuel Vilas-Varela − *Centro Singular de Investigación en Química Biolóxica e Materiais Moleculares (CiQUS) and Departamento de Química Orgánica, Universidade de Santiago de Compostela, 15782 Santiago de Compostela, Spain;* orcid.org/0000-0002-6768-5441

Thomas Y. Baum − *Kavli Institute of Nanoscience, Delft University of Technology, 2628 Delft, The Netherlands;* orcid.org/0000-0003-2802-5384

Niklas Friedrich − *CIC nanoGUNE-BRTA, 20018 Donostia-San Sebastián, Spain;* orcid.org/0000-0001-5353-5680

Francisco Romero-Lara − *CIC nanoGUNE-BRTA, 20018 Donostia-San Sebastián, Spain;* orcid.org/0000-0002-7009-460X

Andrea Aguirre − *Centro de Física de Materiales CSIC/UPV-EHU-Materials Physics Center, 20018 Donostia-San Sebastián, Spain*

Katerina Vaxevani − *CIC nanoGUNE-BRTA, 20018 Donostia-San Sebastián, Spain;* orcid.org/0000-0003-1481-4446

Dongfei Wang − *CIC nanoGUNE-BRTA, 20018 Donostia-San Sebastián, Spain;* orcid.org/0000-0003-4645-2881

Carlos Garcia Fernandez − *Donostia International Physics Center (DIPC), 20018 Donostia-San Sebastián, Spain*

Herre S. J. van der Zant − *Kavli Institute of Nanoscience, Delft University of Technology, 2628 Delft, The Netherlands;* orcid.org/0000-0002-5385-0282

Complete contact information is available at: https://pubs.acs.org/10.1021/acsnano.4c01963

Notes

The authors declare no competing financial interest.

A previous version of this manuscript has been deposited on a preprint server.[53]

ACKNOWLEDGMENTS

The authors gratefully acknowledge financial support from the Spanish MCIN/AEI/10.13039/501100011033 and the European Regional Development Fund (ERDF) through grants PID2022-140845OB-C61, PID2022-140845OB-C62, PID2020-115406GB-I00, and the Maria de Maeztu Units of Excellence Program CEX2020-001038-M, from the European Union (EU) through the FET-Open project SPRING (863098), the ERC Synergy Grant MolDAM (951519), the ERC-AdG CONSPIRA (101097693), and from the Xunta de Galicia (Centro singular de investigación de Galicia accreditation 2019-2022, ED431G 2019/03 and Oportunius Program). F.R.-L. acknowledges funding by the Spanish Ministerio de Educación y Formación Profesional through the PhD scholarship No. FPU20/03305.

REFERENCES

(1) de Oteyza, D. G.; Frederiksen, T. Carbon-based nanostructures as a versatile platform for tunable π-magnetism. *J. Phys.: Condens. Matter* **2022**, *34*, No. 443001.

(2) Das, S.; Wu, J. Polycyclic Hydrocarbons with an Open-Shell Ground State *Phys. Sci. Rev.* 2017, *25* .

(3) Li, J.; Sanz, S.; Corso, M.; Choi, D. J.; Peña, D.; Frederiksen, T.; Pascual, J. I. Single spin localization and manipulation in graphene open-shell nanostructures. *Nat. Commun.* **2019**, *10*, No. 200.

(4) Mishra, S.; Beyer, D.; Eimre, K.; Ortiz, R.; Fernández-Rossier, J.; Berger, R.; Gröning, O.; Pignedoli, C. A.; Fasel, R.; Feng, X.; Ruffieux, P. Collective All-Carbon Magnetism in Triangulene Dimers. *Angew. Chem., Int. Ed.* **2020**, *59*, 12041−12047.

(5) Mishra, S.; Beyer, D.; Eimre, K.; Kezilebieke, S.; Berger, R.; Gröning, O.; Pignedoli, C. A.; Müllen, K.; Liljeroth, P.; Ruffieux, P.; Feng, X.; Fasel, R. Topological frustration induces unconventional magnetism in a nanographene. *Nat. Nanotechnol.* **2020**, *15*, 22−28.

(6) Sugawara, T.; Matsushita, M. M. Spintronics in organic π-electronic systems. *J. Mater. Chem.* **2009**, *19*, 1738−1753.

(7) Naber, W. J. M.; Faez, S.; van der Wiel, W. G. Organic spintronics. *J. Phys. D: Appl. Phys.* **2007**, *40*, No. R205.

(8) Frisenda, R.; Gaudenzi, R.; Franco, C.; Mas-Torrent, M.; Rovira, C.; Veciana, J.; Alcon, I.; Bromley, S. T.; Burzurí, E.; van der Zant, H. S. J. Kondo Effect in a Neutral and Stable All Organic Radical Single Molecule Break Junction. *Nano Lett.* **2015**, *15*, 3109−3114.

(9) Rajca, A. Organic Diradicals and Polyradicals: From Spin Coupling to Magnetism? *Chem. Rev.* **1994**, *94*, 871−893.

(10) Lehmann, J.; Gaita-Ariño, A.; Coronado, E.; Loss, D. Quantum computing with molecular spin systems. *J. Mater. Chem.* **2009**, *19*, 1672−1677.

(11) Sanvito, S. Molecular spintronics. *Chem. Soc. Rev.* **2011**, *40*, 3336−3355.

(12) Shil, S.; Bhattacharya, D.; Misra, A.; Klein, D. J. A high-spin organic diradical as a spin filter. *Phys. Chem. Chem. Phys.* **2015**, *17*, 23378−23383.

(13) Fukuda, K.; Nagami, T.; Fujiyoshi, J.-y.; Nakano, M. Interplay between Open-Shell Character, Aromaticity, and Second Hyperpolarizabilities in Indenofluorenes. *J. Phys. Chem. A* **2015**, *119*, 10620−10627.

(14) Lombardi, F.; Ma, J.; Alexandropoulos, D. I.; Komber, H.; Liu, J.; Myers, W. K.; Feng, X.; Bogani, L. Synthetic tuning of the quantum properties of open-shell radicaloids. *Chem* **2021**, *7*, 1363−1378.

(15) Dong, S.; Li, Z. Recent progress in open-shell organic conjugated materials and their aggregated states. *J. Mater. Chem. C* **2022**, *10*, 2431−2449.

(16) Popp, F.; Bickelhaupt, F.; Maclean, C. The electronic structure of chichibabin's hydrocarbon. *Chem. Phys. Lett.* **1978**, *55*, 327−330.

(17) Montgomery, L. K.; Huffman, J. C.; Jurczak, E. A.; Grendze, M. P. The molecular structures of Thiele's and Chichibabin's hydrocarbons. *J. Am. Chem. Soc.* **1986**, *108*, 6004−6011.

(18) Zeng, Z.; Sung, Y. M.; Bao, N.; Tan, D.; Lee, R.; Zafra, J. L.; Lee, B. S.; Ishida, M.; Ding, J.; Navarrete, J. T. L.; Li, Y.; Zeng, W.; Kim, D.; Huang, K.-W.; Webster, R. D.; Casado, J.; Wu, J. Stable Tetrabenzo-Chichibabin's Hydrocarbons: Tunable Ground State and Unusual Transition between Their Closed-Shell and Open-Shell Resonance Forms. *J. Am. Chem. Soc.* **2012**, *134*, 14513−14525.

(19) Baum, T. Y.; Fernández, S.; Peña, D.; van der Zant, H. S. J. Magnetic Fingerprints in an All-Organic Radical Molecular Break Junction. *Nano Lett.* **2022**, *22*, 8086−8092.

(20) Zuo, L.; Ye, L.; Li, X.; Xu, R.-X.; Yan, Y.; Zheng, X. Unraveling the Nature of Spin Coupling in a Metal-Free Diradical: Theoretical Distinction of Ferromagnetic and Antiferromagnetic Interactions. *J. Phys. Chem. Lett.* **2024**, *15*, 5761−5769.

(21) Huang, Z.; Zhang, Y.; He, Y.; Song, H.; Yin, C.; Wu, K. A chemist's overview of surface electron spins. *Chem. Soc. Rev.* **2017**, *46*, 1955−1976.

(22) Junghoefer, T.; Gallagher, N. M.; Kolanji, K.; Giangrisostomi, E.; Ovsyannikov, R.; Chassé, T.; Baumgarten, M.; Rajca, A.; Calzolari,

A.; Casu, M. B. Challenges in Controlled Thermal Deposition of Organic Diradicals. *Chem. Mater.* **2021**, *33*, 2019−2028.
(23) Eisenhut, F.; Kühne, T.; García, F.; Fernández, S.; Guitián, E.; Pérez, D.; Trinquier, G.; Cuniberti, G.; Joachim, C.; Peña, D.; Moresco, F. Dodecacene Generated on Surface: Reopening of the Energy Gap. *ACS Nano* **2020**, *14*, 1011−1017.
(24) Frota, H. O. Shape of the Kondo resonance. *Phys. Rev. B* **1992**, *45*, No. 1096.
(25) Ternes, M. Spin Excitations and Correlations in Scanning Tunneling Spectroscopy. *New J. Phys.* **2015**, *17*, No. 063016.
(26) Kondo, J. Resistance Minimum in Dilute Magnetic Alloys. *Prog. Theor. Phys.* **1964**, *32*, 37−49.
(27) Ternes, M.; Heinrich, A. J.; Schneider, W.-D. Spectroscopic manifestations of the Kondo effect on single adatoms. *J. Phys.: Condens. Matter* **2009**, *21*, No. 053001.
(28) Li, J.; Sanz, S.; Castro-Esteban, J.; Vilas-Varela, M.; Friedrich, N.; Frederiksen, T.; Peña, D.; Pascual, J. I. Uncovering the Triplet Ground State of Triangular Graphene Nanoflakes Engineered with Atomic Precision on a Metal Surface. *Phys. Rev. Lett.* **2020**, *124*, No. 177201.
(29) Hirjibehedin, C. F.; Lutz, C. P.; Heinrich, A. J. Spin Coupling in Engineered Atomic Structures. *Science* **2006**, *312*, 1021−1024.
(30) Hieulle, J.; Castro, S.; Friedrich, N.; Vegliante, A.; Lara, F. R.; Sanz, S.; Rey, D.; Corso, M.; Frederiksen, T.; Pascual, J. I.; Peña, D. On-Surface Synthesis and Collective Spin Excitations of a Triangulene-Based Nanostar. *Angew. Chem., Int. Ed.* **2021**, *60*, 25224−25229.
(31) Ortiz, R.; Fernández-Rossier, J. Probing local moments in nanographenes with electron tunneling spectroscopy. *Prog. Surf. Sci.* **2020**, *95*, No. 100595.
(32) Hieulle, J.; Fernandez, C. G.; Friedrich, N.; Vegliante, A.; Sanz, S.; Sánchez-Portal, D.; Haley, M. M.; Casado, J.; Frederiksen, T.; Pascual, J. I. From Solution to Surface: Persistence of the Diradical Character of a Diindenoanthracene Derivative on a Metallic Substrate. *J. Phys. Chem. Lett.* **2023**, *14*, 11506−11512.
(33) Song, S.; Solé, A. P.; Matěj, A.; Li, G.; Stetsovych, O.; Soler, D.; Yang, H.; Telychko, M.; Li, J.; Kumar, M.; Chen, Q.; Edalatmanesh, S.; Brabec, J.; Veis, L.; Wu, J.; Jelinek, P.; Lu, J. Highly entangled polyradical nanographene with coexisting strong correlation and topological frustration. *Nat. Chem.* **2024**, *16*, 938−944.
(34) Paaske, J.; Rosch, A.; Wölfle, P.; Mason, N.; Marcus, C. M.; Nygård, J. Non-equilibrium singlet−triplet Kondo effect in carbon nanotubes. *Nat. Phys.* **2006**, *2*, 460−464.
(35) Sanz Wuhl, S.; Papior, N.; Brandbyge, M.; Frederiksen, T. hubbard: v0.4.1. 2023; DOI: 10.5281/zenodo.4748765.
(36) Papior, N. sisl: v0.14.4.dev46+g8754d4f5. 2023; DOI: 10.5281/zenodo.597181.
(37) Rezaei, H.; Phirouznia, A. Modified spin-orbit couplings in uniaxially strained graphene. *Eur. Phys. J. B* **2018**, *91*, No. 295.
(38) Rubio-Verdú, C.; Sarasola, A.; Choi, D.-J.; Majzik, Z.; Ebeling, R.; Calvo, M. R.; Ugeda, M. M.; Garcia-Lekue, A.; Sánchez-Portal, D.; Pascual, J. I. Orbital-selective spin excitation of a magnetic porphyrin. *Commun. Phys.* **2018**, *1*, No. 15.
(39) Jacob, D.; Fernández-Rossier, J. Theory of intermolecular exchange in coupled spin-1/2 nanographenes. *Phys. Rev. B* **2022**, *106*, No. 205405.
(40) Yu, H.; Heine, T. Magnetic Coupling Control in Triangulene Dimers. *J. Am. Chem. Soc.* **2023**, *145*, 19303−19311.
(41) Heinrich, B. W.; Ehlert, C.; Hatter, N.; Braun, L.; Lotze, C.; Saalfrank, P.; Franke, K. J. Control of Oxidation and Spin State in a Single-Molecule Junction. *ACS Nano* **2018**, *12*, 3172−3177.
(42) Vaxevani, K.; Li, J.; Trivini, S.; Ortuzar, J.; Longo, D.; Wang, D.; Pascual, J. I. Extending the Spin Excitation Lifetime of a Magnetic Molecule on a Proximitized Superconductor. *Nano Lett.* **2022**, *22*, 6075−6082.
(43) Heersche, H. B.; de Groot, Z.; Folk, J. A.; van der Zant, H. S. J.; Romeike, C.; Wegewijs, M. R.; Zobbi, L.; Barreca, D.; Tondello, E.; Cornia, A. Electron Transport through Single Mn_{12} Molecular Magnets. *Phys. Rev. Lett.* **2006**, *96*, No. 206801.
(44) Naghibi, S.; Sangtarash, S.; Kumar, V. J.; Wu, J.-Z.; Judd, M. M.; Qiao, X.; Gorenskaia, E.; Higgins, S. J.; Cox, N.; Nichols, R. J.; Sadeghi, H.; Low, P. J.; Vezzoli, A. Redox-Addressable Single-Molecule Junctions Incorporating a Persistent Organic Radical. *Angew. Chem., Int. Ed.* **2022**, *61*, No. e202116985.
(45) Lokamani, M.; Kilibarda, F.; Günther, F.; Kelling, J.; Strobel, A.; Zahn, P.; Juckeland, G.; Gothelf, K. V.; Scheer, E.; Gemming, S.; Erbe, A. Stretch Evolution of Electronic Coupling of the Thiophenyl Anchoring Group with Gold in Mechanically Controllable Break Junctions. *J. Phys. Chem. Lett.* **2023**, *14*, 5709−5717.
(46) Corso, M.; Ondráček, M.; Lotze, C.; Hapala, P.; Franke, K. J.; Jelínek, P.; Pascual, J. I. Charge Redistribution and Transport in Molecular Contacts. *Phys. Rev. Lett.* **2015**, *115*, No. 136101.
(47) Farinacci, L.; Ahmadi, G.; Reecht, G.; Ruby, M.; Bogdanoff, N.; Peters, O.; Heinrich, B. W.; von Oppen, F.; Franke, K. J. Tuning the Coupling of an Individual Magnetic Impurity to a Superconductor: Quantum Phase Transition and Transport. *Phys. Rev. Lett.* **2018**, *121*, No. 196803.
(48) Trivini, S.; Ortuzar, J.; Vaxevani, K.; Li, J.; Bergeret, F. S.; Cazalilla, M. A.; Pascual, J. I. Cooper Pair Excitation Mediated by a Molecular Quantum Spin on a Superconducting Proximitized Gold Film. *Phys. Rev. Lett.* **2023**, *130*, No. 136004.
(49) Horcas, I.; Fernández, R.; Gómez-Rodríguez, J. M.; Colchero, J.; Gómez-Herrero, J.; Baro, A. M. WSXM: A software for scanning probe microscopy and a tool for nanotechnology. *Rev. Sci. Instrum.* **2007**, *78*, No. 013705.
(50) Ruby, M. SpectraFox: A free open-source data management and analysis tool for scanning probe microscopy and spectroscopy. *SoftwareX* **2016**, *5*, 31−36.
(51) Frisch, M. J.; Trucks, G. W.; Schlegel, H. B.; Scuseria, G. E.; Robb, M. A.; Cheeseman, J. R.; Scalmani, G.; Barone, V.; Petersson, G. A.; Nakatsuji, H.; Li, X.; Caricato, M.; Marenich, A. V.; Bloino, J.; Janesko, B. G.; Gomperts, R.; Mennucci, B.; Hratchian, H. P.; Ortiz, J. V.; Izmaylov, A. F.et al. *Gaussian 16*, Revision C.01; Gaussian Inc.: Wallingford CT, 2016.
(52) Soler, J. M.; Artacho, E.; Gale, J. D.; García, A.; Junquera, J.; Ordejón, P.; Sánchez-Portal, D. The SIESTA method for ab initio order-N materials simulation. *J. Phys.: Condens. Matter* **2002**, *14*, 2745−2779.
(53) Vegliante, A.; Fernandez, S.; Ortiz, R.; Vilas-Varela, M.; Baum, T.; Friedrich, N.; Romero-Lara, F.; Aguirre, A.; Vaxevani, K.; Wang, D.; Garcia, C.; van der Zant, H. S. J.; Frederiksen, T.; Peña, D.; Pascual, J. I. Tunning the Spin Interaction in Non-planar Organic Diradicals Through Mechanical Manipulation, arXiv:2402.08641. arXiv.org e-Print archive, 2024, https://arxiv.org/abs/2402.08641. (accessed August 10, 2024).